Expected Background in the LZ Experiment

Vitaly A. Kudryavtsev[1]

for the LZ Collaboration

[1]*Department of Physics and Astronomy, University of Sheffield, Sheffield S3 7RH, UK*

Abstract. The LZ experiment, featuring a 7-tonne active liquid xenon target, is aimed at achieving unprecedented sensitivity to WIMPs with the background expected to be dominated by astrophysical neutrinos. To reach this goal, extensive simulations are carried out to accurately calculate the electron recoil and nuclear recoil rates in the detector. Both internal (from target material) and external (from detector components and surrounding environment) backgrounds are considered. A very efficient suppression of background rate is achieved with an outer liquid scintillator veto, liquid xenon skin and fiducialisation. Based on the current measurements of radioactivity of different materials, it is shown that LZ can achieve the reduction of a total background for a WIMP search down to about 2 events in 1000 live days for 5.6 tonne fiducial mass.

INTRODUCTION

The LUX-ZEPLIN (LZ) experiment will exploit a discrimination power of nuclear recoil against electron recoil events in liquid xenon (LXe) combined with a large fiducial mass, accurate position reconstruction and additional background rejection capabilities offered by several veto detectors. The core of the LZ detector will be a two-phase xenon time projection chamber (TPC) with 7 tonnes of LXe viewed by 488 photomultiplier tubes (PMTs) from top and bottom. A particle interaction in LXe will produce a prompt scintillation signal, S1, as well as ionisation. An electric field of 0.7 kV/cm will drift ionisation electrons towards the gas phase. Electrons will then be extracted into the gas phase where they produce the secondary scintillation, S2. The ratio of the two signals S2/S1 provides discrimination between nuclear recoils (NR) and electron recoils (ER). The time delay between them will give the depth position within the TPC with an accuracy of better than 1 mm. Position in the horizontal plane will be reconstructed with an accuracy of about 1 cm for the smallest signals by measuring the distribution of light in different PMTs. The TPC is enclosed in a PTFE field cage with embedded electrodes and is surrounded by a layer of LXe skin also viewed by PMTs and used as a veto system. Additional vetoing of background events is achieved with a scintillator surrounding the cryostat. Finally, all these systems are embedded into the existing water tank currently used by the LUX experiment. The schematic diagram of the LZ detector is shown in Figure 1 [1].

The LZ experiment is expected to reach a sensitivity to WIMP-nucleon spin-independent interactions down to 2×10^{-12} pb for 50 GeV WIMP mass, limited by the dominant background of astrophysical neutrinos. The neutrino background is primarily due to solar pp-neutrinos producing ER events which can be misidentified as NRs. In addition, coherent scattering of atmospheric and diffuse supernova neutrinos will give NR events. The rate of neutrino events is shown in Table 2 with more details given in [1]. Below we will focus on the background from radioactivity and cosmic rays. A carefully developed background suppression strategy includes: 1) placing the detector deep underground to eliminate most cosmic-ray muons; 2) shielding the target LXe by a sufficient thickness of water, scintillator and LXe; 3) using radio-pure materials in the detector construction; 4) purifying xenon to remove potential radioactive contaminants including those due to cosmogenic activation; 5) exploiting the good position reconstruction to reject multiple hit events; 6) carefully selecting the fiducial volume of LXe to optimise the sensitivity; 7) rejecting events in coincidence with the LXe skin, outer liquid scintillator and instrumented water Cherenkov detector; 8) using the S2/S1 ratio to select NR event candidates.

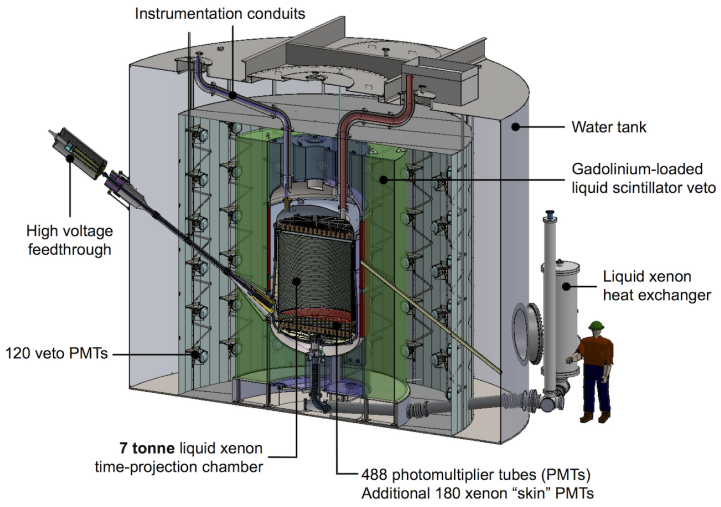

FIGURE 1. Schematic diagram of the LZ detector [1] (http://lz.lbl.gov).

RADIOACTIVITY IN DETECTOR COMPONENTS

With significant shielding around the cryostat (the thickness of water and scintillator is > 160 g/cm^2) and a high background rejection factor due to fiducialisation, multiple hit rejection and veto efficiency, the background from radioactivity in the laboratory environment will not contribute to the event rate in the detector, and events from detector components close to LXe and intrinsic LXe contaminations will dominate the radioactive background. We are carrying out detailed Monte Carlo of neutrons and gamma-rays from these sources and the preliminary results are shown below.

Neutrons caused by the radioactivity are produced in spontaneous fission (mainly ^{238}U) and (α, n) reactions. Neutron yields and spectra from (α, n) reactions and spontaneous fission have been calculated using the modified code SOURCES4 [2]. The code library has been extended to 10 MeV alpha energy and now contains cross-sections of (α, n) reactions and transition probabilities to excited states for most isotopes relevant to low-background experiments (see [3] and references therein). Where experimental data were not found, cross-sections and branching ratios were calculated with the code EMPIRE2.19 [4]. Neutron energy spectra from titanium, PTFE and ceramics (Al_2O_3) are shown in Figure 2 (left). Neutron yields and mean energies are given in Table 1.

To evaluate the background from radioactivity in different components, two methods for neutrons and gamma-rays were used. Neutrons were sampled according to their energy spectra from SOURCES4 and a starting position within particular detector components, and transported through the detector using the LZSim MC code originally developed for the LUX experiment [5] and based on GEANT4 [6]. Their hits in different sensitive volumes of the detector (main xenon target, LXe skin and scintillator veto) have been recorded. To calculate the event rate from gamma-rays and other particles (X-rays, alphas, betas and low-energy electrons), radioactive nuclei of ^{238}U, ^{232}Th, ^{40}K and ^{60}Co were uniformly distributed within the relevant volume and allowed to decay. This resulted in the emission of all particles from the whole decay chain. Again, the energy and positions of hits in different sensitive volumes have been recorded. Initial simulations have been focused on components that are expected to give the highest background due to their high mass (cryostat), potentially higher radioactivity levels (PMTs) and higher neutron production rate (PTFE), assuming secular equilibrium in the U/Th decay chains. Recently the simulations have been extended to the sub-dominant contributors to the background budget and the early and late sub-chains have been normalised separately according to available measurements of decay rates with HPGe detectors and mass-spectrometry results. Decay rates for normalisations have been taken from the LZ screening campaign (if such data were available) or from published results from other measurements. Table 2 gives a snapshot of backgrounds from major sources assuming secular equilibrium. Detailed results will be published in the Conceptual Design Report (CDR) [1]. The LZ Collaboration has began a large material screening campaign involving several HPGe detectors in different underground laboratories, mass-spectrometry and other techniques to characterise materials and components to be used in the LZ construction.

TABLE 1. Neutron production rates due to (α, n) reactions in different materials. The U and Th decay chains were assumed to be in secular equilibrium. The rates are given per kg of material per year per ppb of U/Th concentration. The spontaneous fission of ^{238}U gives a rate of 0.427 neutrons/kg/year for 1 ppb of natural uranium independently of the material. The mean energy of neutrons from spontaneous fission is 1.69 MeV. The column 'Composition' gives the chemical composition of the material sample used to calculate neutron spectra with the abundance of elements (by the number of atoms) given in brackets. Only elements with abundances greater than 1% are shown.

Material	Composition (abundance %)	Neutron yield, $(\text{kg}\cdot\text{y}\cdot\text{ppb})^{-1}$		$< E >$, MeV	
		U	Th	U	Th
Titanium	Ti (100)	0.805	0.679	1.59	1.88
Alumina	Al (40), O (60)	2.60	1.32	1.51	1.62
Quartz	Si (33), O (67)	0.502	0.221	1.94	1.99
PTFE	C (33), F (67)	27.5	11.0	1.60	1.76
Polyethylene	H (67), C (33)	0.452	0.177	3.82	3.70
Stainless steel	Cr (17), Mn (0.02), Fe (69), Ni (12)	0.155	0.182	1.29	1.56
Copper	Cu (100)	0.00981	0.0306	0.584	0.769
Aluminium	Al (100)	5.33	2.71	1.51	1.63
Cirlex	H (26), C (56), N(5), O(13)	0.614	0.261	3.07	2.92
Epoxy	H (44), C (37), N(13), O(6)	0.776	0.369	2.23	2.17

The results from this screening campaign will be used for more accurate calculations of predicted backgrounds. Figure 2 (right) displays example energy spectra of nuclear recoils from the titanium cryostat for different fiducialisation cuts showing a very efficient self-shielding of LXe.

An important feature of the LZ experiment is the anti-coincidence systems which include LXe skin and the Outer Detector; the latter features 21 tonnes of Gd-loaded liquid scintillator contained in transparent acrylic vessels, viewed by PMTs installed in the water space. The LXe skin is efficient at rejecting gamma-ray events originated in detector components, whereas outer liquid scintillator doped with Gd is effective at tagging neutron captures on Gd as well as reducing the external backgrounds. Figure 3 (left) shows the reduction of events by the various anti-coincidence systems. The fiducial volume is defined on the plots as that containing fewer than 1 NR event in 1000 live days (50% efficiency for NR detection is applied) and less than 10% ER events from detector components compared to neutrino-induced events (the former do not include internal contamination of the xenon). The optimised fiducial volume increases significantly (from 3.3 tonnes to 5.6 tonnes) when both veto systems are used. Figure 3 (right) shows the percentage of events surviving different cuts for nuclear (top) and electron (bottom) recoils.

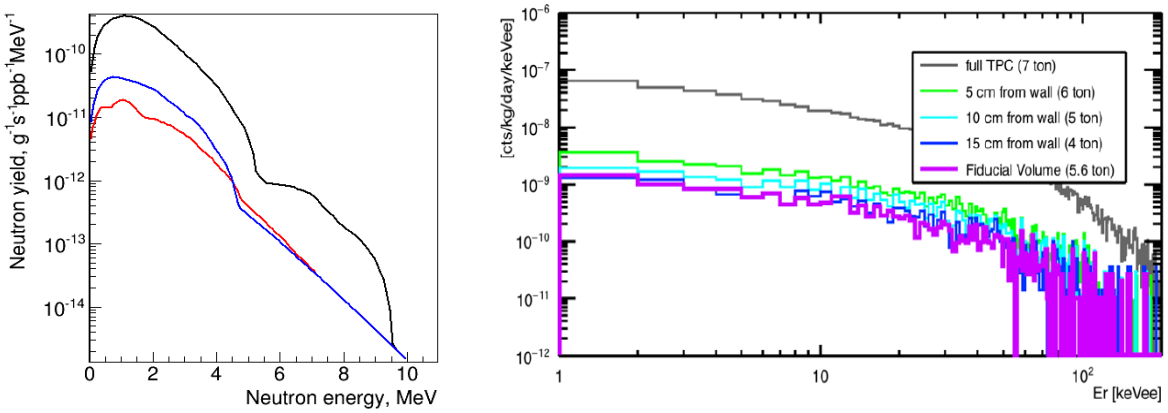

FIGURE 2. Left: Neutron energy spectra from U decay chain in PTFE (black), Ti (red) and Al_2O_3 (blue). The high-energy exponential tails of the spectra are dominated by fission neutrons. Higher neutron yield in PTFE is due to the high cross-section of (α, n) reactions on fluorine. Right: Energy spectra of nuclear recoils from neutrons originated in the cryostat for different fiducial volumes. The optimised volume of 5.6 t of LXe (pink histogram) was chosen to contain the maximum volume of LXe while reducing the total background down to the required level (see text for details).

TABLE 2. Snapshot of the expected number of background events from different components in a 5.6 tonne fiducial mass of LZ in 1000 days, for 1.5-6.5 keV (ER) and 6-30 keV (NR) energy ranges. Columns 3-6 show radioactive contaminations in mBq per kg or per unit as specified in column 2. Column 7 gives neutron production rate per year per kg for given radioactive contaminations. Last two columns show ER (1.5-6.5 keV) and NR (6-30 keV) counts in 5.6 t fiducial mass in 1000 days of running. The row 'internal' contains estimated contributions from ^{nat}Kr (0.015 ppt), ^{222}Rn (0.67 mBq), ^{220}Rn (0.07 mBq), ^{39}Ar (2.7 mBq). Subtotal and total include also a small contribution from other components not shown in the table. The last row includes 99.5% rejection of ER events and 50% efficiency for NR acceptance.

Component	Mass or number	U	Th	^{60}Co	^{40}K	n/kg/year	ER counts	NR counts
TPC PMTs	488 units	0.46	1.3	1.2	17	0.18	4.2	0.36
Ti cryostat	1645 kg	0.62	0.61	0	2.48	0.16	4.1	0.07
PTFE	260 kg	0.01	0.002	0	0.06	0.03	0.1	0.006
TPC PMT bases	488 units	0.36	0.03	0.03	0.03	0.10	1.37	0.19
Cables	60 kg	17	13	11	0	1.8	1.0	0.03
Skin PMTs	180 units	0.32	0.23	1.7	8.6	0.04	0.17	0.03
Liquid scintillator	21000 kg	0.74	0.81	0	0	0.09	0.94	0.005
Acrylic tanks	4100 kg	0.04	0.1	0	0	0.27	0.05	0.0005
Internal							52	
Subtotal							66	0.70
Neutrinos							234	0.61
Total							300	1.31
After discrimination							1.55	0.66

INTERNAL CONTAMINATIONS

To achieve the projected sensitivity, the LZ experiment can tolerate a maximum ^{222}Rn activity within the LXe volume of 0.67 mBq, which corresponds to a steady-state population of approximately 300 atoms. This rate is dominated by the beta-decay of ^{214}Pb to ^{214}Bi, whereas the ^{214}Bi beta-decay is identified by the subsequent ^{214}Po alpha-decay that would be observed within an LZ event waveform ($T_{1/2}$=160 μs). Similar coincidence rejection also occurs where beta-decay is accompanied by a high-energy gamma-ray, which may still be tagged by the LXe skin or external Gd-LS vetoes even if it leaves the active Xe volume. The ^{220}Rn decay chain produces ^{212}Pb, which gives another Bi-Po coincidence (beta-alpha delayed coincidence) similar to ^{214}Pb. Radon daughters are identified through their alpha decay signatures, as demonstrated in LUX [7], and can be used to characterise the ^{222}Rn and ^{220}Rn decay chain rates and distributions in the active region. There are multiple potential sources of radon emanation and a radon emanation screening campaign is planned with a sensitivity down to about 30 μBq for major detector components.

Another intrinsic contaminant in the LXe is ^{85}Kr, a beta-emitter with a half-life of 10.8 years and a dominant beta-decay mode of endpoint energy 687 keV. It is produced in the atmosphere by cosmogenic activation and is also a fission product. It can become a significant contaminant during production and storage of Xe. The research-grade Xe procured for LUX contained on average 130 ppb ^{nat}Kr/Xe with an estimated ^{85}Kr concentration of 2×10^{-11} g/g. To control its contribution to the background budget in LZ, its concentration in the LXe should be kept below 0.015 ppt which will be achieved using chromatography prior to underground deployment. The quantity of argon containing beta-emitting ^{39}Ar with a 269 year half-life and 565 keV endpoint energy, should be less than 10% of ^{85}Kr, resulting in a requirement of < 2.6 μBq. The Kr removal system will also remove Ar.

MUON-INDUCED NEUTRONS

Muon simulations for LZ have been carried out for the Davis campus at SURF located at the 4850 ft level. Initially, muons with different energies at the surface were transported through various thicknesses of rock using MUSIC [8, 9]. The resulting spectra of surviving muons have been convolved with muon spectra at the surface for different zenith angles and slant depths. Figure 4 (left) shows azimuthal angle distribution of muons at Davis campus at SURF

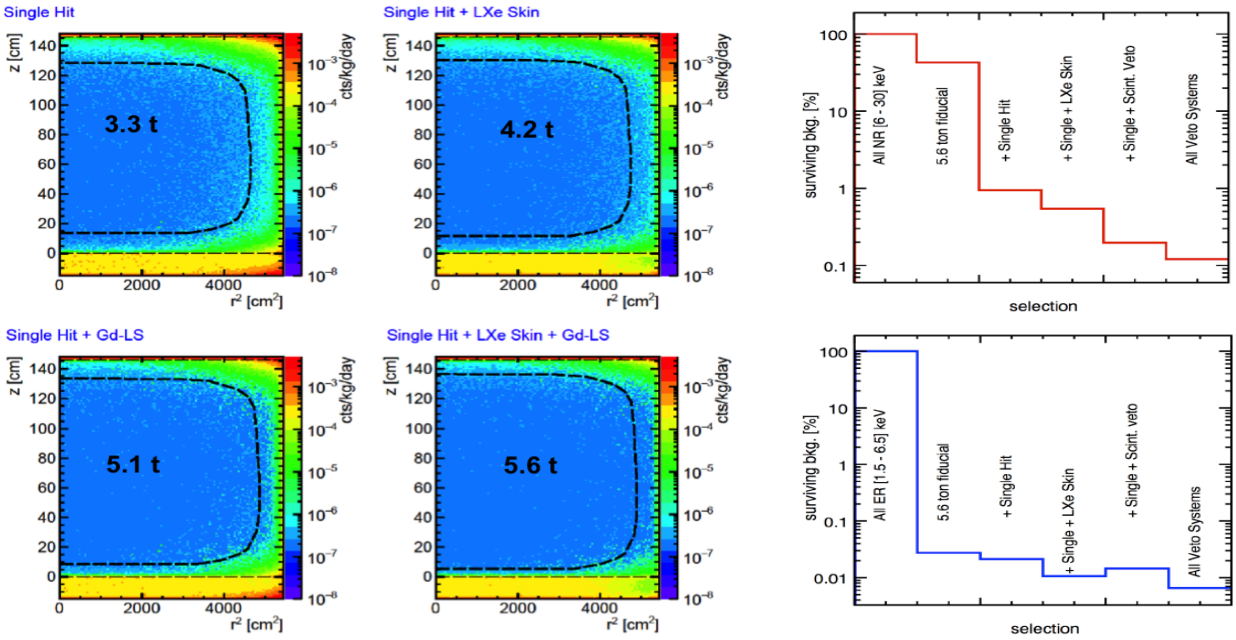

FIGURE 3. Left: Temperature map of background position for single hits in the target xenon volume in the energy range of interest showing progressive reduction of events from veto systems. For electron recoil events a discrimination factor of 99.5% has been applied. Right: Percentage of surviving events after each cut for nuclear recoils (top) and electron recoil (bottom).

integrated over the zenith angle. Peaks and dips on the plot correspond to the dips and peaks in the surface profile above the underground laboratory. Underground muons have been sampled on the surface of a box which contained the cavern and 5-7 m of rock around the cavern using the MUSUN code [8, 9] and transported through the rock and the detector using LZSim. All particles have been followed and their hits in LXe and liquid scintillator recorded. Usual cuts on energy deposition, hit multiplicity, fiducial volume and an anti-coincidence with LXe skin and scintillator veto system have been applied. Figure 4 (right) shows the spectra of nuclear recoils in the 5.6 t fiducial volume of LXe for 58 years of running. No event survives the cuts applied in the analysis which allows us to set a 90% CL upper limit on the muon-induced background rate in LZ of 0.11 events in 1000 live days.

COSMOGENIC ACTIVATION

The irradiation of xenon by cosmic rays at the surface produces a number of radioactive isotopes including those of Xe, tritium, ^{134}Cs, ^{125}I, ^{121m}Te, ^{123m}Te, etc. Non-xenon isotopes will be efficiently removed from the xenon during purification. Among radioactive isotopes of xenon, the most dangerous is ^{127}Xe with a half-life of 36.4 days. Other radioactive xenon isotopes will decay quickly and will not pose any threat after a few months of commissioning and calibration runs. They will also serve as important calibration sources in these early runs. LUX measurements [7] showed 2.7 ± 0.5 mBq/kg of ^{127}Xe decays in xenon exposed to cosmic rays at the Earth's surface. This can be a factor of 3-4 higher if xenon is stored on the surface at SURF (at about 1600 m elevation). Electron capture of ^{127}Xe is accompanied by the emission of X-rays, gamma-rays and electrons, which, in most cases, will give an energy deposition in xenon well above the range of interest (ROI). Escaping high-energy gammas may be tagged by their energy deposition in LXe skin and outer liquid scintillator. LUX data showed that 0.115 mBq/kg of ^{127}Xe produced a background single hit rate of 0.5×10^{-3} events/kg/day/keV in the ROI. The initial ER background in LZ after cuts at 1.5-6.5 keV is expected to be 13 events per day. After 8 months of cooling down time underground this rate drops by two orders of magnitude to 0.13 events/day or a few events in 1000 live days (before discrimination). The early purchase of xenon and storage underground, will allow an early start of the science run.

The most dangerous isotope due to activation of titanium (used to manufacture the cryostat and many internal detector components) is ^{46}Sc (half-life is 83.8 days). We have calculated that titanium exposed to cosmic rays at sea-

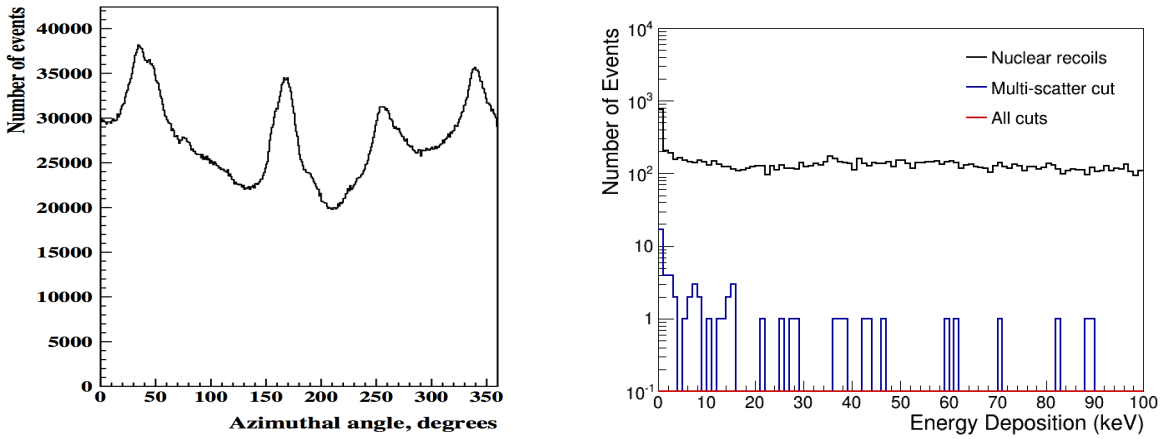

FIGURE 4. Left: Azimuthal angle distribution of muons in the underground laboratory that will host the LZ detector. Azimuthal angle is measured from East to anticlockwise. Right: Spectrum of energy depositions from nuclear recoils in caused by muon-induced neutrons LZ before and after cuts.

level will, after 6 months of activation, contain ^{46}Sc resulting in a decay rate of 2.4 mBq/kg. This is consistent with measurements from LUX [7]. The beta-decay of ^{46}Sc is almost always followed by the emission of two gamma rays, of energies 1120 keV and 889 keV. We expect that, after 8 months of cooling, activated ^{46}Sc will contribute less than 1 event (before discrimination) in 1000 day run of LZ.

CONCLUSIONS

The first simulations and estimates of the LZ background from radioactivity in xenon, detector components, muon-induced neutrons and activation show that the total number of background events (after all cuts including NR/ER discrimination) can be limited to about 2 events in 5.6 tonnes of an optimised fiducial volume in 1000 live days. This background will be dominated by neutrinos. A comprehensive radioactivity screening campaign and efficient purification of xenon are foreseen to limit other sources of background to the above projections. The LZ Collaboration will continue to update background estimates as screening results are obtained. The LZ experiment is expected to achieve a sensitivity down to 2×10^{-12} pb to WIMP-nucleon spin-independent interactions for 50 GeV WIMPs.

ACKNOWLEDGMENTS

The LZ Collaboration acknowledges the support from the U.S. Department of Energy (DoE), the U.S. National Science Foundation (NSF), the State of South Dakota, the UK Science and Technology Facilities Council, Fundação para a Ciência e Tecnologia (Portugal) and the Ministry of Education and Science of the Russian Federation.

REFERENCES

[1] LZ Collaboration, Conceptual Design Report (to be published).
[2] W. B. Wilson et. al., SOURCES4A: A Code for Calculating (α, n), Spontaneous Fission, and Delayed Neutron Sources and Spectra, Technical Report LA-13639-MS, Los Alamos (1999).
[3] V. Tomasello, V.A. Kudryavtsev and M. Robinson, *Nucl. Instrum. Meth. A*, **595** (2008) 431.
[4] M. Herman et al., EMPIRE: Nuclear Reaction Model Code System for Data Evaluation, *Nucl. Data Sheets*, **108** (2007) 2655; EMPIRE 2.19 USER'S GUIDE, www.nndc.bnl.gov/empire219/downloads.html.
[5] D.S. Akerib et al., *Nucl. Instrum. Meth. A*, **675** (2012) 63.
[6] S. Agostinelli et al., *Nucl. Instrum. and Meth. A*, **506** (2003).250.
[7] D.S. Akerib et al., *Astropart. Phys.*, **62** (2015) 33.
[8] P. Antonioli, C. Ghetti, E.V. Korolkova, V.A. Kudryavtsev and G. Sartorelli, *Astropart. Phys.*, **7** (1997) 357.
[9] V.A. Kudryavtsev et al., *Comp. Phys. Commun.*, **180** (2009) 339.